ELSEVIER

Earth and Planetary Science Letters 203 (2002) 925–935

EPSL

www.elsevier.com/locate/epsl

Dynamic interaction of cold anomalies with the mid-ocean ridge flow field and its implications for the Australian–Antarctic Discordance

Shu-Chuan Lin [a,b,*], Ling-Yun Chiao [a], Ban-Yuan Kuo [b]

[a] Institute of Oceanography, National Taiwan University, Taipei, Taiwan
[b] Institute of Earth Sciences, Academia Sinica, P.O. Box 1-55 Nankang, Taipei, Taiwan

Received 25 June 2002; received in revised form 29 August 2002; accepted 30 August 2002

Abstract

Negative thermal anomalies beneath a mid-ocean ridge are dynamically isolated from the ambient upwelling and diverging flow field in the asthenosphere whose viscosity is on the order of 5×10^{19} Pa s or less. This study examines on what condition a near-ridge cold anomaly ascends with the upwelling passive flow and spread off-axis. Three-dimensional numerical modeling demonstrates that, for a given magnitude of the cold anomaly, the viscosity of the asthenosphere, the spreading rate and the interference from continental rifting are the dominant controlling factors to the ascent/descent of the anomaly. To overcome the weight of such an anomaly and couple it with the upwelling, either the spreading rate or the asthenospheric viscosity has to be high. In a low viscosity asthenosphere, the cold anomaly also ascends during the early stage of continental rifting due to the enhanced upwelling induced by the thick continental lithosphere. The dynamic interaction between the cold anomaly and the ambient flow renders a transient nature of the subsidence of the seafloor, which may lead to exaggerated temperature variation estimated by using a conduction model alone. The scenarios examined are employed to place a constraint on dynamic models recently proposed for the Australian–Antarctic Discordance, in which the source of the negative anomaly is hypothesized to be deeply rooted in the upper mantle. With the asthenospheric viscosity less than 10^{20} Pa s, the upwelling of the cooler material from great depths, which causes a significant topographic low at the Discordance, is made possible only by rifting of the Australian continent off the Gondwanaland.

Keywords: thermal anomalies; viscosity; dynamic flow; rifting; AAD; subsidence

1. Introduction

The topography of the mid-ocean ridge crest varies by ∼2000 m worldwide [1], suggesting that a heterogeneous temperature along the ridge is the primary cause. The apparent correlation between the axial depth and the subsidence rate of the seafloor implies that the along-ridge segmentation in mantle properties persists with age (e.g. [2]). The prediction of the simple form of the depth–age relationship by using 1-D conductive

* Corresponding author. Tel.: +886-2-2783-9910; Fax: +886-2-2783-9871.
E-mail address: sky@earth.sinica.edu.tw (S.-C. Lin).

0012-821X/02/$ – see front matter © 2002 Elsevier Science B.V. All rights reserved.
PII: S0012-821X(02)00948-2

models [3–4] is consistent with the assumption that what is beneath the ridge propagates downstream with seafloor spreading. However, structures that are thermally different may evolve into dramatically different results in the ridge environment. A ridge segment that is 'hotter' than normal is likely to preserve its properties on- and off-axis as long as the source of the anomaly remains, because the hot anomaly is self-buoyant and dynamically preferable in the upwelling and diverging environment [5,6]. A relatively cold mantle section beneath the ridge, however, has to work against its own weight in the ascending mantle, being an unstable process that takes place only under appropriate conditions. If the segmentation along the ridge is long-lived, including temperature variations, then a quantitative examination of these conditions may shed light on the dynamics of the mid-ocean spreading center.

The mid-ocean ridge structure is dominated by convection of 3-D flow, and is usually modeled separately from the static, conduction-dominated off-axis region. In the past, modeling efforts have been directed at increasing the degree of complexity of the 3-D flow field of a 'normal' spreading center to explain various geophysical and geochemical observations (e.g. [7]). How a near-ridge thermal structure sets out to propagate off-axis remains to be explored. In this study we document systematically the conditions on which a cold anomaly, e.g. 150°C lower than the ambient temperature, survives the interaction between its own weight and the ambient upwelling. We demonstrate that a temperature- and pressure-dependent viscosity, with a minimum at upper asthenospheric depths, tends to localize the near-ridge cold anomaly and prevent it from rising and spreading, except for a very high spreading rate (e.g. >10 cm/yr).

We also investigate the role of continental rifting, which is motivated by recent attempts to unravel the cause of the Australian–Antarctic Discordance. It has been argued that the anomalously deep seafloor of the Discordance is caused by the sucking of the ancient slab material trapped in the bottom of the upper mantle by the opening of the Southeast Indian Ocean [8]. We show that, if realistic asthenospheric viscosity is assumed, such a model requires incorporation of the continental lithosphere whose thick 'keel' enhances the upwelling in the spreading center. All the scenarios examined in this study result in anomalous or transient subsidence characteristics that would easily lead to erroneous interpretation in mantle temperature variation if conductive cooling alone is invoked.

2. Method

Our 3-D dynamic model considers thermal convection of Boussinesq fluid of infinite Prandtl number. The non-dimensional equations for continuity, momentum, and energy are, respectively:

$$\nabla \cdot \boldsymbol{u} = 0, \tag{1}$$

$$-\nabla P + \nabla \cdot (\eta(\nabla \boldsymbol{u} + (\nabla \boldsymbol{u})^{\mathrm{T}})) + Ra(T - T_{\mathrm{ref}}/T_0) = 0, \tag{2}$$

$$T_t + \boldsymbol{u} \cdot \nabla T - \nabla^2 T = 0 \tag{3}$$

where $\boldsymbol{u}$ is the flow velocity vector, P the dynamic pressure (perturbation from the hydrostatic state), η the dynamic viscosity, T the temperature and t the time. The notation $()^{\mathrm{T}}$ indicates the transpose of a second-order tensor. The value chosen for each of these parameters in this study is given in parentheses in the following. T_{ref} (1350°C) is the temperature at which the density ρ is at its reference value of 3300 kg m^{-3}, T_0 is the reference temperature used for temperature non-dimensionalization ($T_0 = T_{\mathrm{ref}}$ in our modeling) and the Rayleigh number $Ra = \rho\alpha g \Delta T d^3/\kappa\eta_0$ is evaluated with the gravitational acceleration g, the coefficient of thermal expansion α (3×10^{-5} K^{-1}), the vertical length scale d (400 km), the characteristic temperature difference ΔT (1350°C), the thermal diffusivity κ (10^{-6} m^2 s^{-1}), and the reference viscosity η_0, an adjustable parameter for different experiments. The mantle viscosity is a function of the temperature T and the lithostatic pressure P, with the form of:

$$\eta(T,P) = \eta_0 \exp[(E+PV)/RT-(E+P_0V)/RT_0] \quad (4)$$

where E (520 kJ mol) is the activation energy, V (10^{-5} m^3 mol^{-1}) the activation volume and R the universal gas constant, and $\eta(T_0, P_0) = \eta_0$ with P_0 the hydrostatic pressure at 100 km. The viscosity usually reaches a minimum at mid-asthenospheric depth, and then increases at a rate about 10-fold per 100 km further down. Every 100°C reduction in temperature also increases the viscosity 10-fold. Although still ad hoc, the commonly used values of η_0 range between 10^{18} and 10^{20} Pa s for the upper mantle [7,9]. To ensure the numerical stability, the viscosity is clipped at 10^{18} and 10^{22} Pa s in this study.

The model dimension is 4400 km (x)$\times$6400 km (y)$\times$400 km (z) (Fig. 1), discretized to 90$\times$66 $\times$26 grid nodes. The grid spacings are 50, 100 and 16.7 km in x, y and z directions, respectively.

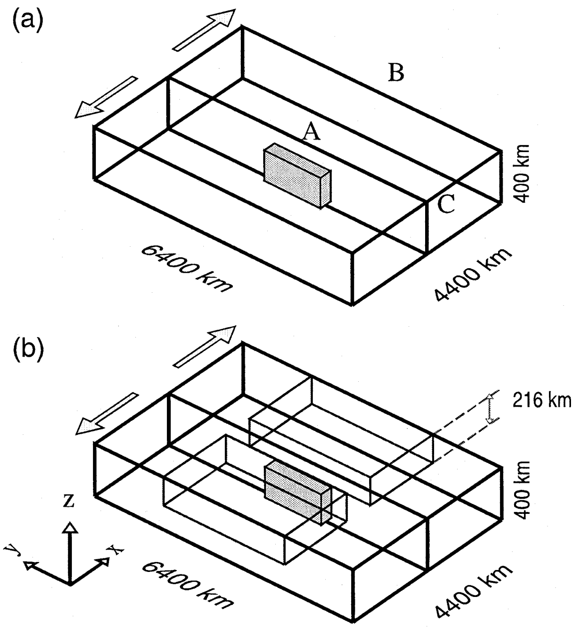

Fig. 1. Geometric configuration of the numerical experiments. (a) Pure oceanic spreading. Arrows indicate the plate divergence. An imposed thermal structure, with cold anomaly of −150°C extending in the depth range of 65–400 km, is marked by the shaded volume. (b) Experiment that incorporates rifting continents with thickness of 216 km, extending into much of the asthenosphere (thin frame cubes).

The large extent in the spreading direction (4400 km) is to ensure the reliable examination of off-axis subsidence behavior at old age, whereas an even larger dimension in the along-ridge direction is to avoid potential complications arising from the interaction between domain boundaries with edges of continents when continent rifting is considered. The top boundary is assigned the spreading velocity of the plate. The y-perpendicular boundaries are symmetric in velocity, and the bottom and the x-perpendicular boundaries are prescribed to be free in buoyancy and dynamic pressure to suppress secondary convection in the thermal boundary layer and to approximate the plate-driven, passive flow solution. All side boundaries are assumed adiabatic, while the temperatures at the top and bottom boundaries are fixed at 0°C and 1350°C, respectively. A 5 Myr old, half-space cooling model with mantle temperature of 1350°C is assigned as the initial condition in the whole calculation domain, including the continental blocks. Only the domain younger than the age under discussion is of interest to us.

Eqs. 1–3 are solved by a primitive variable formulation with finite volume discretization. We employ a modified SIMPLE (semi-implicit pressure-linked equations) algorithm [10] to solve Eqs. 1 and 2. We also use a full multigrid algorithm with a linear nested V-cycle iteration, bilinear interpolation for prolongation operator, and half-weighting for restriction operator [11]. All variables are discretized at the center of each cell. The viscosity is calculated at the center of the cell by Eq. 4, and interpolated to the surrounding cell faces by a harmonic scheme which conserves the continuity of stress better under large viscosity contrast [12]. Velocities are linearly interpolated between the cell center and cell edge.

To solve Eq. 3, the power law method [10] is used for the spatial discretization and predictor–corrector method for time derivatives as in Christensen [13]. SIP (strongly implicit procedure) [14] is used as a smoother for the multigrid solver of Eqs. 1 and 2. Our computational procedure is benchmarked against the 2-D and 3-D natural convection model of Blankenbach et al. [15] and Christensen et al. [16], respectively. We also compare our results with the calculated isotherms reported in Moresi and Solomatov [17] for the cases in which the Rayleigh number is equal to 10^7 and the viscosity contrast up to 10^5.

3. Models

3.1. Effects of buoyancy and plate-driven flow

The cold anomaly in this study is modeled as a columnar structure 1400 km long along the ridge axis, 300 km wide across the ridge, and 65 km below the surface (Fig. 1a). We show below that there is a wide range of geometries of the anomaly within which the ultimate results of the experiments remain effectively the same. In the first experiment, a half-rate plate velocity U of 3.5 cm/yr and an initial thermal anomaly δT of −150°C (T = 1200°C) are specified. The initial temperature at the bottom (400 km) is fixed over time to ensure a long-lived source from below 400 km.

We first examine the case in which $\eta_0 = 5\times10^{19}$ Pa s, which is within the range of acceptable viscosities for shallow oceanic upper mantle [7,9,18]. The 20 Myr snapshot shows that the core (−100°C) of the cold anomaly has collapsed much from its original height (Fig. 2a), resulting from the decoupling of the ambient flow from the more dense body of the anomaly through a relatively low viscosity. The downward dynamic flow driven by the negative buoyancy prevails beneath the center and the plate-driven passive flow bypasses the cold structure when making its way to the ridge axis (Fig. 2b). A pronounced along-

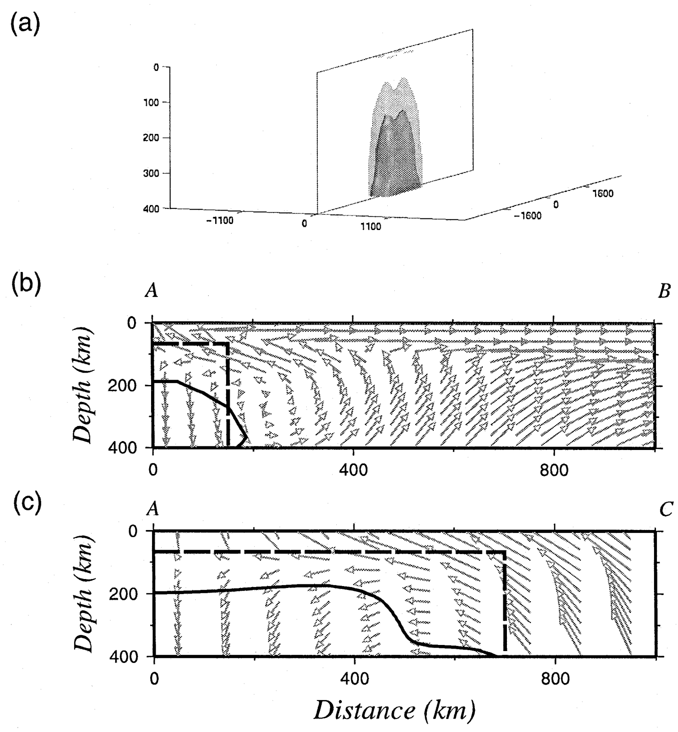

Fig. 2. The first experiment, which shows the collapse of the cold anomaly, or an descending event, with a viscosity η_0 of 5×10^{19} Pa s at the snapshot of 20 Myr. (a) 3-D perspective of isothermal surfaces of −100°C (dark) and −30°C (light), both having collapsed from their original height. The thin line denotes the model domain in the cross-section along ridge. (b) The velocity field (arrows) and the temperature perturbation from the reference state, i.e. a 3-D model without the cold anomaly, in the cross-section AB as denoted in Fig. 1. The arrows near the surface represent 3.5 cm/yr. The contour is the −100°C isotherm (bold line). The dashed-line frame near the ridge outlines the initial geometry of the cold anomaly. (c) Same as in panel b, but in the cross-section AC.

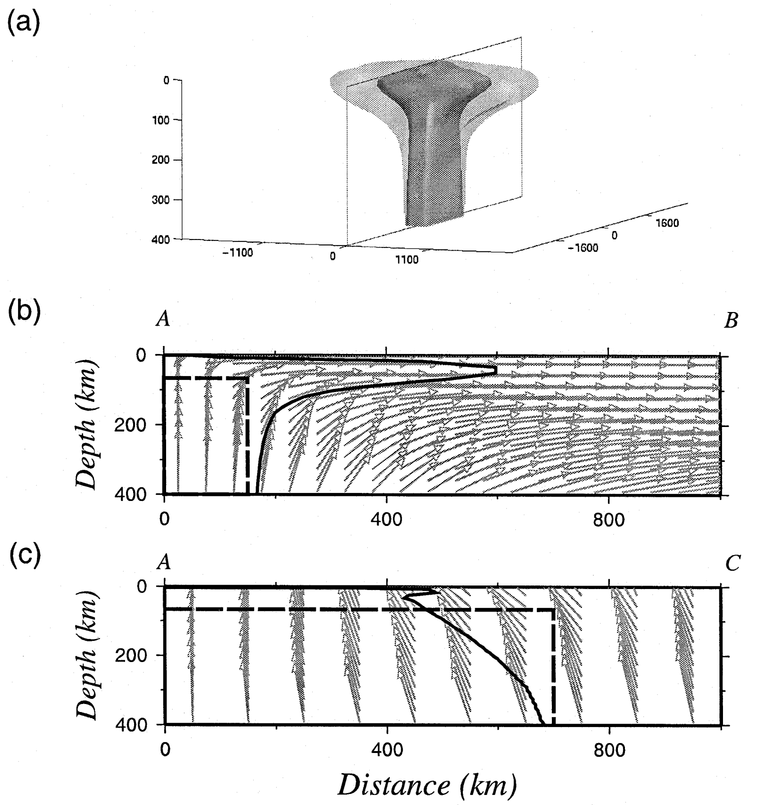

Fig. 3. Example of an ascending scenario with a reference viscosity of 5×10^{20} Pa s. A snapshot at 40 Myr is chosen to highlight the growth of the structure. Both −100 and −30°C isosurfaces reach the surface and spread off-axis (a). The flow field is dominated by the simple upward, plate-driven component (b,c), as opposed to the complex, 3-D dynamic flow shown in Fig. 2b,c.

ridge flow occurs along the ridge (Fig. 2c), apparently driven by the short supply of material from directly below and off-axis for accretion at the spreading center. In comparison, we conducted an experiment with a viscosity 10 times higher than that of the first experiment, showing the result in Fig. 3. Unlike that in Fig. 2, the dynamic flow is dominated by the plate-driven flow, which lifts the core of the cold anomaly to the surface (Fig. 3). For the above two experiments, snapshots at 20 and 40 Myr are chosen to show the temperature and flow field in the middle of the collapse and the growth of the structure, respectively.

To determine what mechanisms control the fate of the cold anomaly, we carried out a series of experiments with δT of −150°C as used above but covering a large range of Rayleigh numbers and spreading rates, two parameters that best characterize the dynamic and kinematic factors of the model. In each experiment with a specific combination of Rayleigh number, or effectively the inverse of η_0, and spreading rate U, the result is labeled as 'ascent' if the cold core (< -100°C) grows to a depth of 50 km in 20 Myr. Otherwise the result is labeled as 'descent'. The result is summarized in Fig. 4. It is appropriate to draw the conclusion at 20 Myr because the ascent/descent scenarios never reverse after this amount of time. The boundary between the two regimes can be modeled by the combination of two straight lines with positive slopes in the parameter space, indicating that the cold anomaly can be drawn up and spread out with either fast spreading or high viscosity. The ascent/descent definition based on −30°C yields a boundary that is indistinguishable

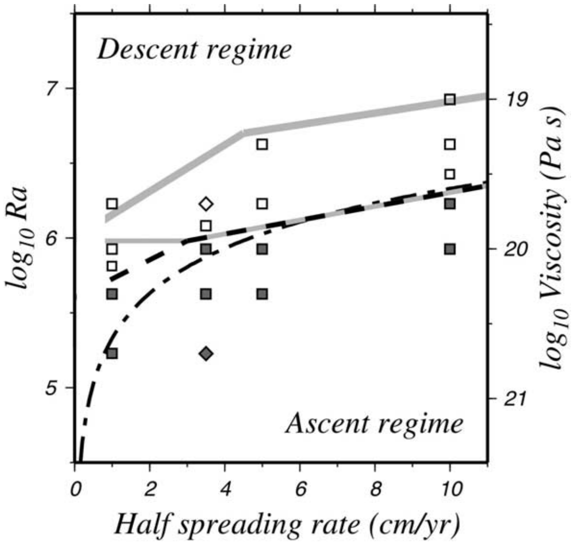

Fig. 4. Division of the ascent versus descent regime in the parameter space of the spreading rate and the mantle viscosity. Filled symbols are cases in which the implanted cold anomalies ascend in our experiments, whereas open symbols represent descending, based on −100°C. The dashed line marks the sharp transition between them. The thin gray line that runs through the dashed line at higher rates represents the transition defined for −30°C. The open diamond at 3.5 cm/yr marks our first experiment of descending (Fig. 2), and the filled diamond represents a 10-fold increase in viscosity and an ascending event (see Fig. 3). The dotted-dashed curve marks the onset of ascending (defined in text) based on the Stokes flow analogy. When the effect of the enhanced upwelling induced by the rifting continents is considered, the ascent–descent boundary is moved to the upper thick gray line, for a duration of about 20 Myr.

from that based on −100°C except at very low velocities (Fig. 4). In the descent regime, the cold anomaly is convectively unstable and short-lived, while in the ascent regime it persists with age and is able to cool the seafloor far off-axis to different extents depending on δT.

The physics responsible for the formation of such a boundary in Fig. 4 is further examined analytically using the Stokes flow formulation [19], in which we parameterize the cold anomaly of −150°C as a dense sphere immersed in a viscous medium. We assume that keeping the dense sphere still in a uniformly upwelling fluid is the prerequisite of ascending, and that the uniform upward velocity of the fluid is $(2/\pi)U$ as defined by the passive flow model for the ridge axis region [20]. The balance between negative buoyancy of the sphere and the viscous drag on its surface yields a curve in the parameter space of η_0 and U, which, according to our definition, marks the onset of ascending. We choose a Stokes sphere with a radius of 70 km to establish a curve that agrees with the one derived from the numerical experiments at high spreading rates. Despite the arbitrary settings in both numerical and analytical estimations, the overall consistency in trend between the two estimates verifies the complementary relationship between the spreading rate and viscosity. The non-diffusive, surface-dragging Stokes sphere strictly follows an $\eta \cdot U$ = constant relationship, which causes a curve deviating significantly from the boundary for a thermal anomaly at low spreading rates.

The ascent–descent boundary in Fig. 4 is insensitive to the detailed geometry of the cold anomaly in the numerical experiment. An anomaly initially spanning from the surface to 400 km has its top 5–10 km propagate coherently with the plate, but the stem below is rapidly eroded away by the flow that converges to feed the axis. Widening the cold body in the spreading direction from 300 to 800 km changes the flow field significantly but does little to the boundary in Fig. 4. Narrowing the structure does not make it less stable until it is too thin because right beneath the axis the lateral erosion is minimal. Shortening the structure sideways is not critical until down to a length of 500 km, when the trimming by the along-axis flow becomes too destructive.

One of the few observables for an ascent event is the change in the rate of subsidence of the seafloor. We calculate the seafloor depth as a function of age for the two models in Figs. 2 and 3, assuming that mantle columns are in isostatic equilibrium in the upper 200 km, which is deep enough for our model ages. The subsidence curves for the 1-D conduction model in the form of $d = d_0 + 2[(\alpha\rho_m T_m)/(\rho_m - \rho_w)](\kappa/\pi)^{1/2}(t)^{1/2}$, with initial mantle temperatures T_m of 1350 and 1200°C, are provided as references for normal and slow subsidence, respectively. In the above expression, d_0 is the predicted zero-age depth and t the age of the lithosphere [3]. The curve for each T_m is posi-

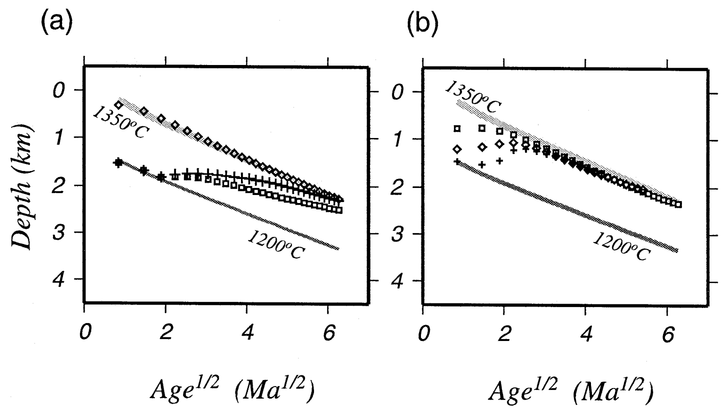

Fig. 5. Seafloor subsidence manifested from thermal contraction. (a) In spite of the initial presence of the cold anomaly, the subsidence (open diamonds) with the normal reference viscosity (5×10^{19} Pa s) is indistinguishable from what is predicted from the simple cooling model without the anomaly ($T_m = 1350°C$, light gray line). With η_0 raised to 5×10^{20} Pa s, the cold material is able to influence the off-axis subsidence (crosses), and at 40 Myr the seafloor mimics the subsidence character that can be explained by a conductive cooling model of $T_m = 600°C$. The 60 Myr seafloor (squares) shows even more approaching the 1200°C curve. (b) Crosses, diamonds, and squares represent snapshots of subsidence after spreading for 20, 30, and 40 Myr when the rifting continents are incorporated (see Fig. 6).

tioned at d_0 (0 and 1.29 km for 1350 and 1200°C, respectively) at age zero. For a descent event in which the cold fails to cool the lithosphere, the subsidence of the seafloor with age is identical to that predicted by the idealized 1-D analytical model with $T_m = 1350°C$ (Fig. 5a), and the corridor reveals no sign of unusual properties of the mantle. Notice that the subsidence for the ascent event in Fig. 3 exhibits a temporal variation. The subsidence starts with a characteristic curve representing a T_m of 1350°C, now at 40 Myr, but gradually converges to that of $T_m = 1200°C$ near the ridge. Given longer time, the curve will settle at the 1200°C curve.

3.2. Effect of continental breakup and the implication for the Australian–Antarctic Discordance

The opening of the thick continental lithosphere that accompanies the opening of an oceanic spreading center disturbs the flow and modifies the scenarios summarized in Fig. 3. The work in this section is motivated by the recent discussion of the formation of the Australian–Antarctic Discordance (AAD), a segment between roughly 115 and 120°E on the Southeast Indian Ridge (SEIR). The deep and rugged seafloor of AAD has been thought to manifest a cooler than normal mantle section (e.g. [21]). Quantitative modeling points to a δT on the order of $-100°C$ in shallow upper mantle and a retarded upwelling [22], and the opening of the SEIR as the key mechanism for shaping the isotopic and topographical variations along the ridge [23]. Recently, Gurnis et al. [8] proposed that the slab trapped in the mantle transition zone during a subduction from the Cretaceous convergent boundary between the Pacific and Gondwanaland is the source of the cool material. In their nominal model, this cool material was drawn from the source to the surface to generate the thin crust and the dynamic topography at AAD. This nominal model has a simple viscosity structure, i.e. 10^{21} Pa s for the upper mantle sandwiched between a 100 km thick lithosphere and a half-space lower mantle at 660 km, both of which have a 10^{23} Pa s viscosity. In essence, a low viscosity asthenosphere is absent.

The 'slab' in their model since 60 Ma is characterized by a δT of -100 to $-200°C$ and the rising material 'a few tens of degrees' cooler than normal, making appropriate the direct examination against our $-30°C$ ascent–descent boundary in Fig. 4. The high viscosity in Gurnis et al.'s [8] model facilitates an ascent event, in contrast to our first experiment, which resides in

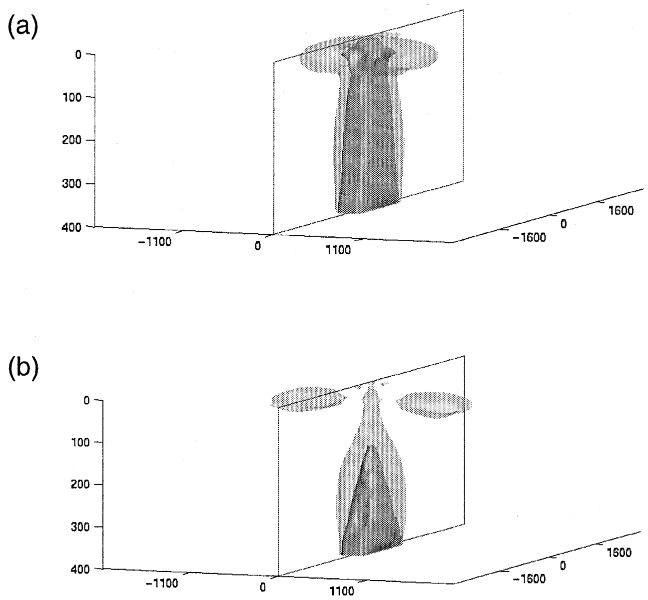

Fig. 6. Evolution of the cold anomaly during continental rifting. Isosurfaces are the same as in Figs. 2 and 3. (a) After 20 Myr, the cold core has reached the surface. (b) The core collapses at 40 Myr as the continents drift away and the additional drive of flow diminishes.

the descent regime with a lower and more realistic viscosity (Fig. 4). Here we examine an alternative mechanism relevant to AAD, that is, rifting between Australia and Antarctica. Both continents are Paleozoic or Archean in age (e.g. [24]), and probably have a 'keel' that is 200–250 km thick as discerned by seismic velocity (e.g. [25]).

Two blocks of high viscosity, bearing an initial dimension of 1900 km (x)$\times$3000 km (y)$\times$216 km (z), are imposed in the oceanic model configuration to represent the continental lithosphere (Fig. 1b). To compare with the first experiment, we use $U = 3.5$ cm/yr, and $\eta_0 = 5\times10^{19}$ Pa s. The first 20–30 Myr of rifting is dominated by the coherent translation of the massive continental keel inducing a pressure gradient that favorably drives more upwelling behind the keel or near the ridge. Fig. 6a shows that even the cold core is stretched to the surface and just about to propagate laterally. With the boost from the keel, the ascent–descent boundary is pushed upward temporarily toward lower viscosity (Fig. 4) to furnish an ascent event with η_0 of 5×10^{19} Pa s. However, the excess upwelling dies out with time as the continents drift further apart (Fig. 7). After 40 Myr the bulk of the cold structure collapses (Fig. 6b) and the ascent–descent boundary curve resumes its pure oceanic spreading position (Fig. 4). The resultant subsidence reveals a time-dependent feature (Fig. 5b).

4. Discussion

This study skips the problem of why and how an anomalous mantle section exists in the first place beneath a spreading center. The cold anomaly portrayed in this study may be derived from the paleoslab, as proposed for the AAD region [8], or represent a remnant of the mantle after a ridge jump. Another example of a possible cold spot on ridge is the Pacific–Antarctic ridge [2,26], but its origin has not been fully investigated. Trench rollback may cause the slab to be trapped in the transition zone [27], becoming a potential source of cold material, whereas the spreading in the back arc environment is too sluggish to lift the cold unless the viscosity is 2×10^{20} Pa s or higher according to Fig. 4.

The transient nature of the subsidence, or the

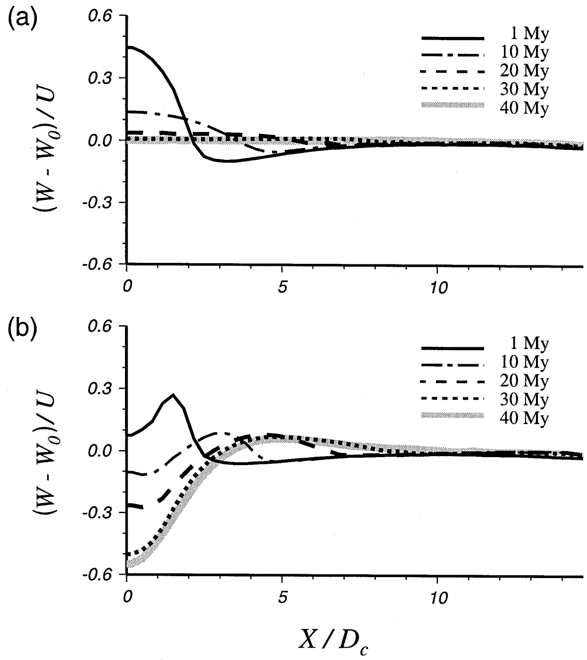

Fig. 7. Decay of continental effect with time on driving the upwelling near the ridge. The magnitude of vertical velocity at 200 km depth is plotted against the distance from the ridge axis. (a) Continental rifting, without the presence of the thermal anomaly. The velocity is referenced to the flow field of a pure oceanic model W_0, and normalized by the plate velocity U, and the horizontal scale is normalized by the width of the cold anomaly D_c. Continental rifting produces larger vertical flow than oceanic spreading for at least the first 20 Myr, which helps raise the cold. (b) The same as panel a, but with the cold anomaly. The velocity distribution here is effectively superimposing on the field in panel a, the collapsing of the cold anomaly in the no-spreading surface condition. The net flow is still positive until after probably 20 Myr.

non-linearity of the depth–age$^{1/2}$ curve (Fig. 5), results partly from the setup of the model, i.e. it takes time for the anomaly 65 km down below to reach the surface. However, one point highlighted by the experiments is that different subsidence rates are very likely to appear for different age intervals. The fitting to the entire curve for the high viscosity experiment (Fig. 5a) would result in a subsidence rate of 165 m/Myr$^{1/2}$, corresponding to a T_m of 600°C, which might thus lead to an estimate of 750°C variation in T_m rather than the actual 150°C. A similarly exaggerated temperature variation estimate may result from the seafloor 'data' as shown in Fig. 5b if a conduction-only model is applied to a short range of seafloor ages.

We have reduced the complexity of the model by ignoring the effect of compositional buoyancy that has been widely examined in the study of mid-ocean ridge dynamics [7,28]. By first order estimation, 5% depletion of the residual mantle contributes to the compositional buoyancy equivalent to +100°C thermal perturbation. A simple inference is that partial melting is suppressed in the cold region but occurs mostly in the region above it, for our particular setting of the model. A few factors should be considered to estimate how melting might alter our results. First, melting increases buoyancy of the residual mantle above the cold anomaly and enhances the upward advection. Secondly, water extraction during melting may lead to high viscosity in mantle residue [29], increasing the coupling and favoring an ascending scenario. Consideration of the above effects effectively relaxes the condition for ascending.

For the upper mantle of the AAD region, another complicating factor stems from its possible origin as a mantle wedge. It is hypothesized that ancient subduction of the Pacific slab under Gondwanaland might have formed a mantle wedge before it turned to a divergent environment in the Late Cretaceous [30,31], and this wedge may be low in viscosity due to water or even melt retention. The reduction of viscosity hinders ascending, contrary to the effects discussed above. Modeling these complicated and probably still controversial factors is challenging but beyond the scope of the present paper.

We do not directly confront data to create a new model for AAD, but instead examine previous models in the context of the ascent–descent tectonics as summarized in Fig. 4. We point out the negative effect of a less viscous asthenosphere in maintaining continuous advection from the deeply rooted source to the surface. In Gurnis et al.'s [8] model, which integrates the regional tectonic history and various geophysical and geochemical observations, the viscosity structure is simplified to exclude a pressure- and temperature-dependent viscosity, and the uniform viscosity they used is probably too high [7,9,18]. A more realistic rheology can be incorporated into this model to throw new light on the cause of the AAD and the role of continental rifting. The continental effect as modeled here lasts roughly 20 Myr, which is almost half of the duration over which the spreading of SEIR picked up the rate of 3.5 cm/yr after an initial phase of sluggish breakup. The 20 Myr episode of cooling due to continental rifting therefore may be more important than it appears to the subsidence history of SEIR. Furthermore, despite its short time of impact, it produces a thin crust that would have been frozen in the lithosphere to maintain the topographic low. Further quantification of the role of continental rifting in the regional tectonics of AAD requires investigation utilizing a more sophisticated model than the generalized one in this study.

5. Conclusions

The fate of the cold anomaly beneath a mid-ocean spreading center reflects the balance between dynamic and kinematic forces that dominate this tectonic setting. Viscosity, spreading rate, and continental rifting all compete to determine whether the cold anomaly should ascend with the upwelling mantle or collapse by its own negative buoyancy. Either high viscosity or fast spreading is required to maintain an ascent event in which cold material reaches the surface through continuous advection. Rifting of a 200 km thick continental lithosphere, however, is comparable to increasing the viscosity five-fold in the early stage of continental breakup. The rifting scenario is relevant to the recent model of the cause of AAD. At a half-rate as low as 3.5 cm/yr for SEIR, this study demonstrates that the cold material rooted below 400 km cannot be drawn up to cool the lithosphere and thin the crust at AAD, as this previous model proposed, if there exists a low viscosity asthenosphere. To facilitate an ascent scenario in the AAD region, rifting of the Australian continent from Gondwana, both of which probably have a thick 'keel', may have played a positive role. The combination of these various factors yields transient or non-linear seafloor subsidence variations, which leads to an overestimation of temperature variation across corridors if a 1-D analytical conduction model is employed.

Acknowledgements

We thank Louis Moresi and an anonymous reviewer for their careful and constructive reviews of the manuscript. This research was supported by the National Science Council of Taiwan, Republic of China, under Grants NSC 90-2611-002-002 and NSC 90-2116-M-001-016.*[AC]*

References

[1] P. Calcagno, A. Cazenave, Subsidence of the seafloor in the Atlantic and Pacific Oceans: Regional and large-scale variations, Earth Planet. Sci. Lett. 126 (1994) 473–492.
[2] D.E. Hayes, K.A. Kane, Long-lived mid-ocean ridge segmentation of the Pacific-Antarctic ridge and the Southeast Indian ridge, J. Geophys. Res. 99 (1994) 19679–19692.
[3] E.E. Davies, C.R.B. Lister, Fundamentals of ridge crest topography, Earth Planet. Sci. Lett. 21 (1974) 403–415.
[4] B. Parsons, J.G. Sclater, An analysis of the variations of ocean floor bathymetry and heat flow with age, J. Geophys. Res. 82 (1977) 803–827.
[5] L.Y. Chiao, C.W. Wang, Effect of near-ridge thermal anomalies on the subsidence of the oceanic lithosphere:

Constraints from a 2-D dynamic model, Geophys. Res. Lett. 26 (1999) 807–810.
[6] G. Ito, Reykjanes 'V'-shaped ridges originating from a pulsing and dehydrating mantle plume, Nature 411 (2001) 681–684.
[7] D.W. Sparks, E.M. Parmentier, The structure of three-dimensional convection beneath spreading centers, Geophys. J. Int. 112 (1993) 81–91.
[8] M. Gurnis, R.D. Müller, L. Moresi, Cretaceous vertical motion of Australia and the Australian-Antarctic Discordance, Science 279 (1998) 1499–1504.
[9] M.A. Eberle, D.W. Forsyth, Regional viscosity variations, small-scale convection and slope of depth-age$^{1/2}$ curve, Geophys. Res. Lett. 22 (1995) 473–476.
[10] S.V. Patankar, Numerical Heat Transfer and Fluid Flow, Hemisphere, New York, 1982, 197 pp.
[11] W.H. Press, S.A. Teukolsky, W.T. Vetterling, B.P. Flannery, Numerical Recipes, The Art of Scientific Computing, 2nd edn., Cambridge University Press, New York, 1992, 963 pp.
[12] M. Ogawa, G. Schubert, A. Zebib, Numerical simulation of three-dimensional thermal convection in a fluid with strongly temperature-dependent viscosity, J. Fluid Mech. 233 (1991) 299–328.
[13] U.R. Christensen, Convection with pressure- and temperature-dependent non-Newtonian rheology, Geophys. J. Astron. Soc. 89 (1984) 343–384.
[14] J.H. Ferziger, M. Peric, Computational Methods for Fluid Dynamics, Springer, New York, 1996, 356 pp.
[15] B.F. Blankenbach, U. Christensen, L. Cserepes, D. Gunkel, U. Hansen, H. Harder, G. Jarvis, M. Koch, G. Marquart, D. Moore, P. Olson, H. Schmeling, T. Schnaubelt, A benchmark comparison for mantle convection codes, Geophys. J. Int. 98 (1989) 23–38.
[16] U.R. Christensen, H. Harder, 3-D convection with variable viscosity, Geophys. J. Int. 104 (1991) 213–226.
[17] L.-N. Moresi, V.S. Solomatov, Numerical investigation of 2D convection with extremely large viscosity variations, Phys. Fluids 7 (1995) 2154–2162.
[18] F.F. Pollitz, R. Bürgmann, B. Romanowicz, Viscosity of oceanic asthenosphere inferred from remote triggering of earthquakes, Science 280 (1998) 1245–1249.
[19] D.L. Turcotte, G. Schubert, Geodynamics, Wiley, New York, 1982, 450 pp.
[20] I. Reid, H.R. Jackson, Oceanic spreading rate and crustal thickness, Mar. Geophys. Res. 5 (1981) 165–172.
[21] J.K. Weissel, D.E. Hayes, The Australian-Antarctic Discordance: new results and implications, J. Geophy. Res. 79 (1974) 2579–2587.
[22] B.Y. Kuo, S.H. Hung, L.Y. Chiao, A 3-D dynamic model for the anomalous topography and geoid over the Southeast Indian Ridge, Geophys. J. Int. 121 (1995) 1–20.
[23] B.P. West, W.S.D. Wilcock, J.-C. Sempéré, L. Géli, Three-dimensional structure of asthenospheric flow beneath the Southeast Indian Ridge, J. Geophys. Res. 102 (1997) 7783–7802.
[24] C. Jaupart, J.C. Mareschal, The thermal structure and thickness of continental roots, Lithos 48 (1999) 93–114.
[25] J. Polet, D.L. Anderson, Depth extent of cratons as inferred from tomographic studies, Geology 23 (1995) 205–208.
[26] L. Géli, H. Bougault, D. Aslanian, A. Briais, L. Dosso, J. Etoubleau, J.L. Formal, M. Maia, H. Odréas, J. Olivet, C. Richardson, K. Sayanagi, N. Seama, A. Shah, I. Vlastelic, M. Yamamoto, Evolution of the Pacific-Antarctic Ridge South of the Udintsev Fracture Zone, Nature 278 (1997) 1281–1284.
[27] R.W. Griffins, R.I. Hackney, R.D. vanderHilst, A laboratory investigation of effects of trench migration on the descent of subducted slabs, Earth Planet. Sci. Lett. 133 (1995) 1–17.
[28] K. Jha, E.M. Parmentier, D.W. Sparks, Buoyant mantle upwelling and crustal production at oceanic spreading centers: On-axis segmentation and off-axis melting, J. Geophys. Res. 102 (1997) 11979–11989.
[29] G. Hirth, D.L. Kohlstedt, Water in the oceanic upper mantle: implications for rheology, melt extraction and the evolution of the lithosphere, Earth Planet. Sci. Lett. 144 (1996) 93–108.
[30] M. Gurnis, R.D. Müller, The origion of the Australian Antarctic Discordance, from an ancient slab and mantle wedge, in: The Evolution and Dynamics of the Australian Plate, to be jointly published by the Geological Societies of Australia and America, 2001, in press.
[31] M.I. Billen, M. Gurnis, A low viscosity wedge in subduction zones, Earth Planet. Sci. Lett. 193 (2001) 227–236.